International Journal of Civil Engineering (2026) 24:195–208
https://doi.org/10.1007/s40999-025-01182-1

RESEARCH PAPER

Allowable Bending Stress for Glass Beams: Experiments and Statistical Analysis

Saddam Hussain[1] · Pei Shan Chen[1] · Chiara Bedon[2] · Hassan Javed[3]

Received: 16 August 2024 / Revised: 26 September 2025 / Accepted: 31 October 2025 / Published online: 22 December 2025

Abstract

A fundamental understanding of resisting and collapse mechanisms is required to ensure the structural safety of primary load-bearing elements, like columns and beams. The present research, in this regard, experimentally investigates the in-plane bending and Lateral-Torsional Buckling (LTB) response of tempered glass beams, analyzing key factors such as the evolution of bending stress, the critical buckling moment, and the corresponding failure mode for a total of 52 original samples. The study focuses on specimens with small slenderness (less than 1.2), revealing that well-defined failure mechanisms can be detected when varying rhis ratio. The stress ratio ($\gamma = 0.57$) is crucial in determining the bending behaviour, with high slenderness following Euler's buckling curve for beams in LTB, but medium- or low-sleenderness specimens exhibiting an inelastic response, with a sudden and brittle collapse mechanism which diverges from Euler's curve, indicating a critical condition for safety. The study identifies three slenderness ratios satisfying specific limits. Statistical analysis is applied to the collected results, revealing that the allowable stress curve begins on the y-axis with an approximate reduction factor of 0.55 and converges with Euler's curve at high slenderness values. As shown, the strategy can be used to correlate the failure type to the slenderness. It could hence provide practical support for improving the safety and efficiency levels of structural glass members. Besides, a more extensive database will be required for a sound and robust calibration of key parameters.

Keywords Glass · Design · Bending · Lateral-torsional buckling (LTB) · Allowable stress

1 Introduction

In architecture, glass has evolved from a secondary building material to a strategic solution for innovation and creativity, contributing to the development of new aesthetic concepts and even complex load-bearing mechanisms [1, 2]. characterised by the progressive minimisation or deletion of supporting metal frames to maximise. Additionally, this transition has been characterised by the progressive minimisation or deletion of supporting metal frames to maximise. Additionally, this transition has been characterised by the progressive minimisation or deletion of supporting metal frames to maximise the transparency of glass [3]. In this sense, the increasing demand for frameless glass structures has promoted a rise in research efforts supporting structural innovation, including the use of tempered glass panels as load-bearing elements [3–5].

To address the challenge of high transparency for spatial structures that can ensure both aesthetic impact and structural efficiency, see, for example, Fig. 1. Chen et al. [5–8]

✉ Chiara Bedon
chiara.bedon@dia.units.it

Saddam Hussain
saddam.hussain372@mail.kyutech.jp

Pei Shan Chen
chen@civil.kyutech.ac.jp

Hassan Javed
hh3887958@gmail.com

[1] Department of Civil Engineering and Architecture, Kyushu Institute of Technology, Kitakyushu, Japan

[2] Department of Engineering and Architecture, University of Trieste, Trieste, Italy

[3] Department of Civil Engineering, Lahore Leads University, Thokar Niaz Baig, Pakistan

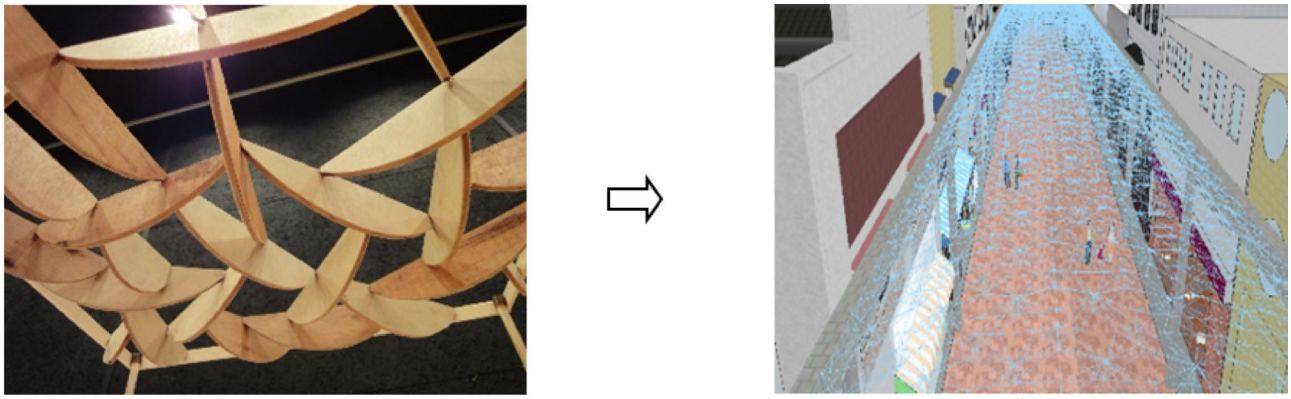

(a) Reciprocal panels emerged from traditional Chinese window grilles

(b) Glass roof of an arcade

Fig. 1 Configuration of frameless glass structure

proposed a solution based on ancient structural principles, inclusive of beam-like members, which play a key role in frameless glass structures. The Lap-beam system [5], more in detail, was inspired by the structural principles of ancient wooden bridges like the Hongqiao, and can represent an innovative solution for modern structural design. The Reciprocal panel system, as shown in Fig. 1, was derived from reciprocal frames that are typical of several cultures and can provide a robust framework for constructing frameless glass structures, combining heritage-inspired design with modern engineering principles [6–8].

The study reported in [6–8] also promoted a process for structural design calculations of frameless structures, including the calibration of allowable stress as shown in Fig. 2, which basically requires, as for most of load bearing members composed of traditional constructional materials [9, 10], that the maximum stress $\sigma_{\max}$ should not exceed the limit:

$$\sigma_{\max} \leq \alpha f_i \tag{1}$$

whit α a sound design safety factor and $f_i$the allowable stress. Specific parameters and considerations are taken into account for different loading conditions, within the consolidated allowable stress design method [9, 10].

The design of members composed of glass, in this context, could be adapted to the allowable stress approach, but necessarily requires a sound calibration of the reference parameters and values that could ensure short-term and long-term safety and durability. For flexural members, as in the present study, the allowable bending stress should be calibrated, but the same concept can be considered for many other loading configurations, such as compression or tension, to guarantee the structural integrity of load-bearing elements made of glass.

For frameless glass domes like in Fig. 1, a preliminary model transformation as in Fig. 2 is also required, which makes the mathematical problem easier to solve and to be adapted to different configurations. A trial structural design is, necessary for each glass member, given that equivalent beams having comparable axial and bending stiffness are taken into account. The design should account for dead and seismic loads, which can be conventionally established according to standards. In similar conditions, the structure can be designed to withstand the maximum stresses due to design loads, preventing it from exceeding the allowable reference value [11].

As shown in the following sections, the presently discussed methodology is overall supported by a set of experiments carried out on a total of 52 tempered glass beams. Mechanical properties that are relevant for structural analysis, such as bending response and Lateral-Torsional Buckling (LTB) capacity, are evaluated. The performed experimental investigation, in this sense, aligns with Eurocode theory [12] and earlier literature efforts on LTB [13–19], and supports a more detailed study for critical buckling analysis of glass members in pure bending.

The allowable bending stress is successively derived based on the elaboration of experimental results, with statistical analysis. The outcome, as shown, is a set of equations that could be used for calculating the allowable bending stress in general members and could represent a practical tool for safety prevention.

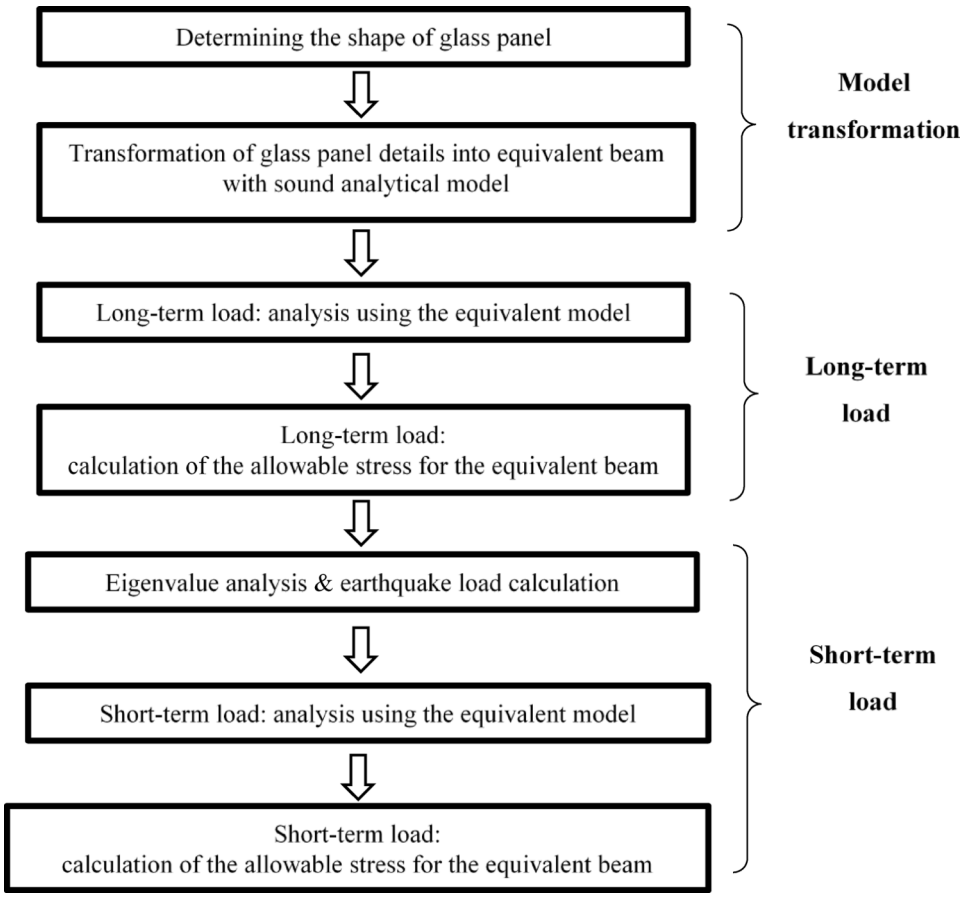

Fig. 2 Structural design processes [11]

2 Background and Previous Studies

According to the literature, several researchers primarily focused on the structural performance assessment of laminated glass members under various loading scenarios, including LTB [13] or other critical conditions for buckling [14]. As a part of spatial domes [11], the supporting glass members can be subjected to in-plane bending and in-plane axial forces. For structural safety and stability purposes [15, 16], the effect of axial forces should be carefully addressed because particularly critical and able to give evidence of in-plane bending or even LTB [17–19]. When in-plane axial loads are applied, the neutral axis of the resisting section moves in fact to the opposite side at equilibrium limits [20], and LTB may manifest itself in the form of large deformations and critical stress peaks [21, 22], and even premature collapse [23].

To detect and mitigate any LTB design criticality, it is thus necessary to address the slenderness of the glass beam to verify [24]. However, the slenderness itself may be insufficient. Whilst the literature offers various simplified strategies, there are still several aspects to address and develop for the optimal calibration of efficient design procedures. Among others, the present study draws attention to the analysis of mechanical properties for laterally unrestrained glass beams in pure bending, and in particular, to the derivation of allowable stress values to prevent failure. Such a goal agrees with standard structural design procedures, where there are several types of allowable stress, including those for bending, compression, tension, and joint failure.

In [25], the authors conducted in-plane loading tests on tempered glass panels to experimentally evaluate the mechanical properties of members in pure compression. The study was extended in [18] to tempered beams under in-plane bending and LTB. As a further extension from previous efforts, the present study aims to evaluate their allowable bending stress, to support the elaboration and calibration of practical design considerations based on the consolidated allowable stress design method, and to adapt it to frameless glass structures.

As illustrated by Fig. 3, the design procedure, as in Fig. 2, is based on the analysis of the pure bending mechanism for an equivalent glass beam, which could result in large bending deflections and even lateral-torsional buckling (LTB) mechanisms for a given critical moment.

The reference beam of Fig. 3 has a h-high × t-thick cross section, l_b effective length, and is composed of glass, with E and G the elastic and shear moduli, respectively.

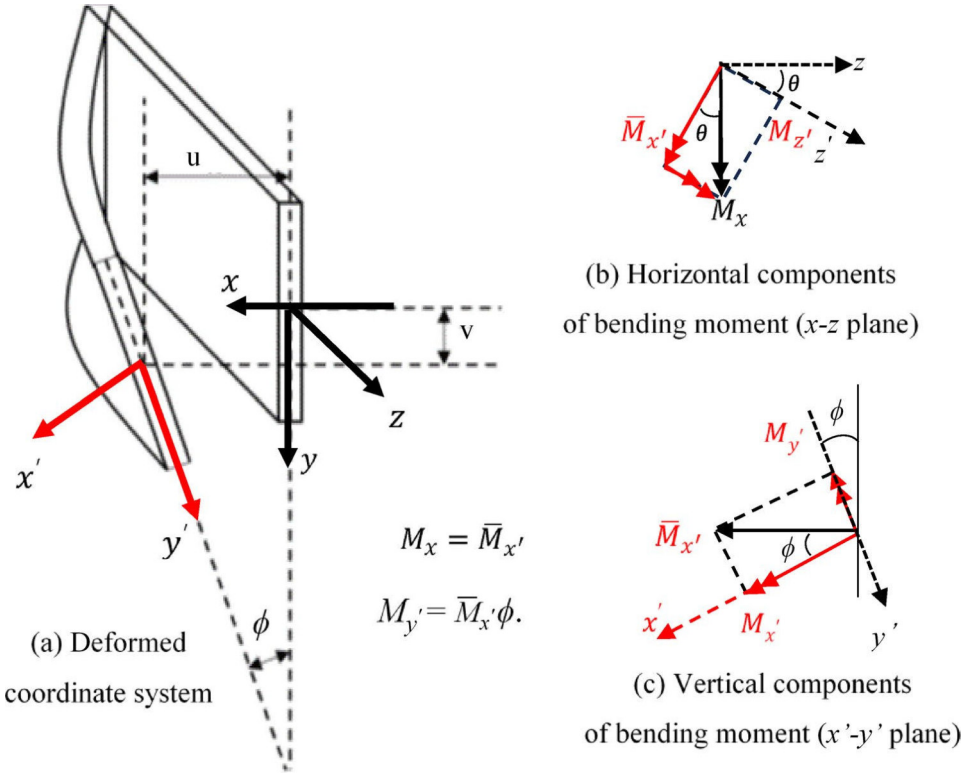

Fig. 3 Lateral deformation of a monolithic beam in LTB

The critical buckling moment for LTB can be obtained from the differential equations of equilibrium, assuming that the positive curvature of the deflected beam axis in Fig. 3 is expressed as d^2u/dz^2 and d^2v/dz^2:

$$EI_x\frac{d^2v}{dz^2} = M_x \quad EI_y\frac{d^2u}{dz^2} = \Phi M_x \quad GJ\frac{d\phi}{dz} = -\frac{du}{dz}M_x \tag{2}$$

Where the bending stiffness parameters (EI_x, EI_y) and the torsional stiffness (GJ) have both a primary role in the beam stability assessment. The Euler's critical moment M_{cr} is in fact conventionally expressed as [12]:

$$M_{cr} = \frac{\pi}{l_b}\sqrt{EI\ GJ} \tag{3a}$$

and for a general boundary and loading configuration, it is:

$$\overline{M}_{cr} = C_b\frac{\pi}{l_b}\sqrt{EI\ GJ} \tag{3b}$$

Where I represents the second moment of the area around the minor axis and J is the torsional moment, while C_b is the moment modification factor. There are several literature attempts to study the moment modification factor and improve the description of the expected LTB behaviour for a general beam setup and boundary/loading configuration [26–30].

As in Eq. (3b), it largely affects the critical bending moment based on boundary conditions, in addition to material properties and geometrical parameters.

A more accurate LTB assessment, however, necessarily requires determining the real maximum bending load (and corresponding failure stress) that the structural member can withstand without losing its integrity and stability. The governing parameter for the realistic estimation of the corresponding LTB capacity is hence represented by the buckling reduction factor, which basically can be estimated for a real member as [14]:

$$\chi_{LT} = \frac{M_{cr}}{M_{res}} \leq 1 \tag{4}$$

an is usually implemented (in empirical form [11]) for the definition of modified buckling curves for design, as a function of the slenderness ratio [12, 14, 16]:

$$\lambda_{LT} = \sqrt{\frac{\sigma_t W_x}{M_{cr}}} \tag{5}$$

with σ_t the tensile strength of glass.

For practical purposes, the effective LTB slenderness (and thus capacity, based on Eq. (4)) is strictly correlated to a combination of parameters of simple determination [14], such as the resisting bending moment ($M_{res} = \sigma_t W_x$) and the elastic modulus of the section ($W_x = ht^2/6$) [15]. A key

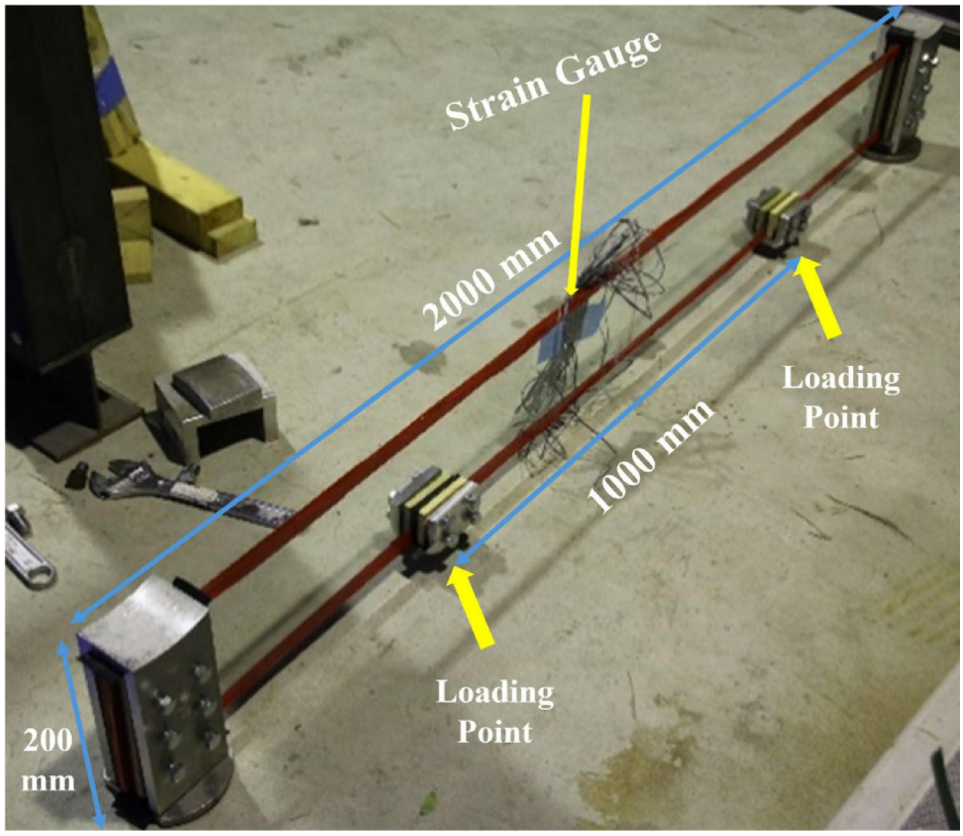

Fig. 4 Experimental sample, restraints and instruments (before testing)

role is indeed assigned to the imperfection coefficients and factors that strictly affect the final χ_{LT} value for the real member object of study [16].

In this context, an important aspect to consider is that for medium-large slenderness ratios, the use of conventional methods and Euler-based buckling theories represents an efficient design approach to manage LTB collapse. Besides, the glass members are characterized by small slenderness (as for the presently examined glass specimens), the failure mechanism is typically associated with an inelastic LTB mechanism a sudden and brittle collapse, which represents a critical condition for safe design.

3 Experimental Program

Given that the purpose of presently reported experiments is to support the determination and calibration of a possible allowable bending stress value for glass beams in bending, it is first crucial to understand the mechanical properties of glass material and beam performance. Failure mechanisms, in this context, are strictly dependent on both the brittle properties of glass and on the possibly high slenderness of the members, where the latter represents a parameter of paramount relevance for LTB considerations. The mutual interaction of material brittleness and member slenderness – in addition to individual influencing parameters – is thus a particularly critical aspect to generally assess and quantify in a univocal way.

Table 1 Geometrical properties of the experimental specimens (52 samples for a single test each; l=2000 mm)

Series	Series label	No. of specimens	Thickness (t) [mm]	Height (h) [mm]
A	TG6-200	4	6	200
	TG8-200	4	8	200
	TG10-200	4	10	200
B	TG8-130	10	8	130
	TG8-150	10	10	150
	TG10-180	10	8	180
	TG12-200	10	12	200

3.1 Test Matrix and Specimens Geometry

The experimental program focused on the LTB mechanism of 52 full-scale specimens, as in Fig. 4; Table 1. Overall, for practical reasons, a uniform length l=2000 mm was taken into account for the tested toughened glass specimens, considering indeed variations in width and thickness.

Until breakage, glass can be handled as a linear elastic material, with Young's modulus E = 70 GPa, Poisson's ratio n = 0.23, and density r = 2500 kg/m³. Besides, the tensile

strength σ_t (with 70 MPa the nominal value of characteristic strength in tension) is a well-known uncertain parameter, which is further affected by many different aspects. Moreover, among others, the bending and LTB response of real glass beams depends on a combination of additional influencing parameters, including the beam shape and aspect ratio – and thus slenderness [14]. While simplified techniques and realistic empirical formulae, such as those in [5], can offer preliminary estimates for the Euler's critical moment and actual LTB capacity of glass beams under various loading configurations, these approaches may take advantage of further insight into some additional important mechanical and geometrical aspects [11].

3.2 Loading Strategy and Measurements

The test frame, schematically shown in Fig. 5, was used for the experimental investigation of the 52 specimens from Table 1. The glass beam specimens were placed under LTB conditions and gradually loaded with two concentrated

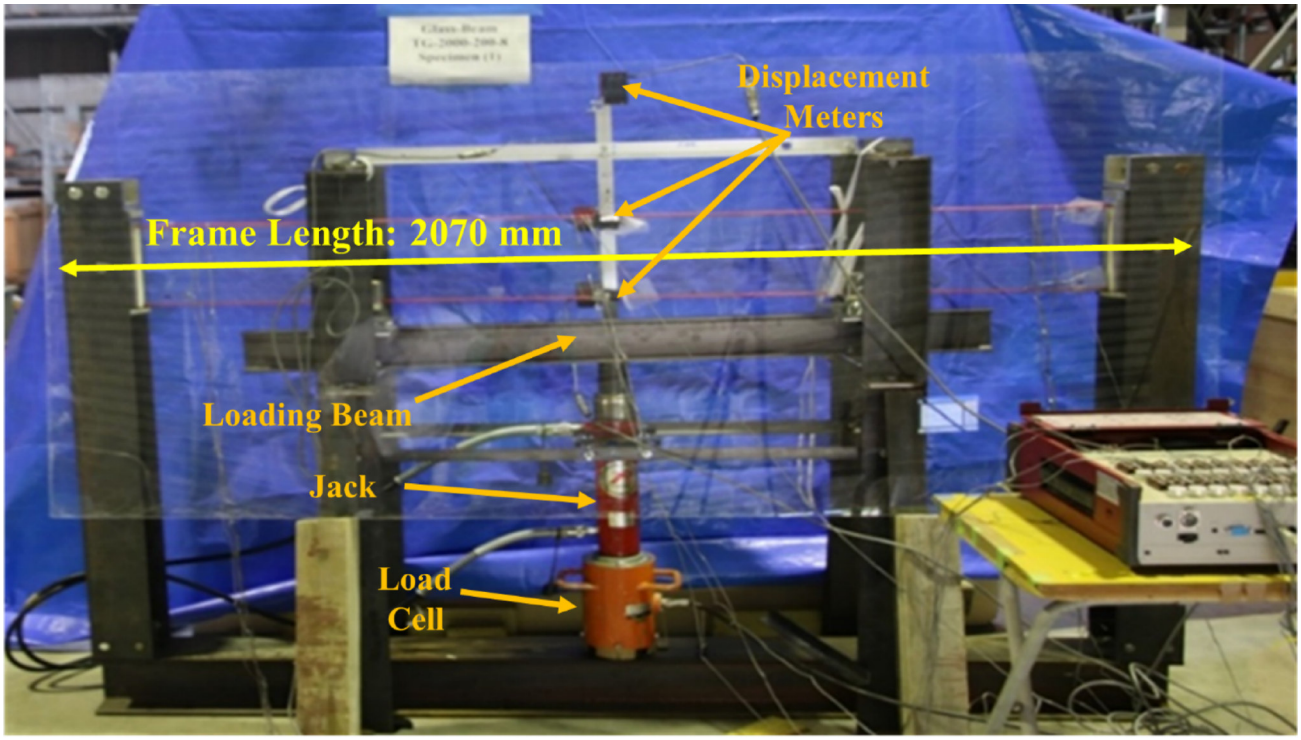

(a) Global view for the setup of the present experimental study

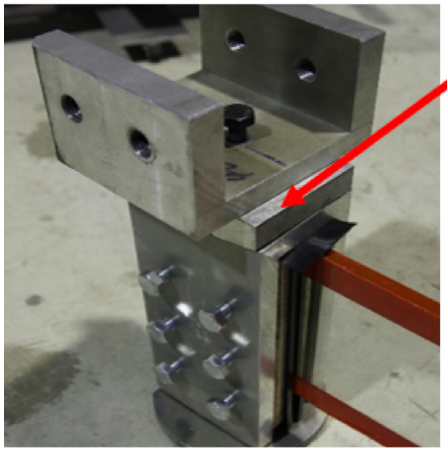

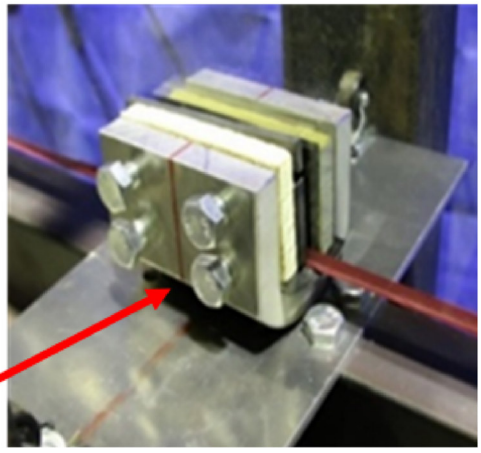

(b) Boundary detail (c) Loading apparatus

Fig. 5 Experimental arrangement

vertical forces. These imposed vertical loads were incrementally increased until a predetermined value was reached in the elastic stage, and then an additional load increment was applied until failure or LTB occurrence.

Instruments for key measures included a load cell with a capacity of 200 kN and wire displacement transducers, with a stroke of 500 mm. The mid-span vertical displacement and lateral twist (due to LTB) of each member were continuously monitored at the top and bottom edges, as a function of the imposed load. In addition, strain gauges were used to measure the top and bottom stresses at the glass edges.

As shown in Fig. 6, the experimental investigation systematically tested both Type A and Type B specimens as in Table 1, under in-plane loading conditions, to assess the consequent out-of-plane bending. Moreover, the study investigated the effect and influence of in-plane axial loading on the structural resisting mechanism of the same glass beams, to find possible correlations in terms of load-bearing capacity, type of collapse, and beam characteristics.

As an example, the collected results for beam specimens with 12 mm thickness are illustrated in Fig. 7, where the in-plane axial loads up to ≈32 kN were applied to reach failure. A negative displacement, like in Fig. 7a, denotes a vertical deflection of the specimen. The basis of the typical trend for the collected records is the pronounced out-of-plane displacement and twist of the member, which was characterized by a failure mechanism consisting of a sudden catastrophic collapse, see Fig. 7d.

For both the vertical and horizontal displacement components reported in Table 2, different rates were measured during tests. The out-of-plane displacement of each member, more precisely, was calculated according to the strain-based method discussed in [18].

Following past literature studies [11, 14, 16], the slenderness λ_{LT} of the tested members is also reported in Table 2. As far as the results for Type A beams are considered, the variation of beam thickness can mostly double the calculated slenderness ratio. The modification of bending and inertial properties is expressed, based on experimental observations, in a more than linearly proportional variation of vertical and horizontal components of displacement. The corresponding failure load follows a similar trend, moving from 6 mm to 10 mm in the A series with fix beam dimensions. Besides, the primary attention of the present investigation is given to Type B specimens, which are characterized by a relatively low slenderness.

The top vertical displacement (Top-ver (v)) is measured using in-plane bending, whereas the horizontal top edge (Hor (u_{top})) and bottom edge (Hor (u_{bot})) displacements assess the lateral twist and buckling of the beam. For the tested specimens, the increase in thickness is combined with variations of width, with a consequent more pronounced reduction of the calculated slenderness.

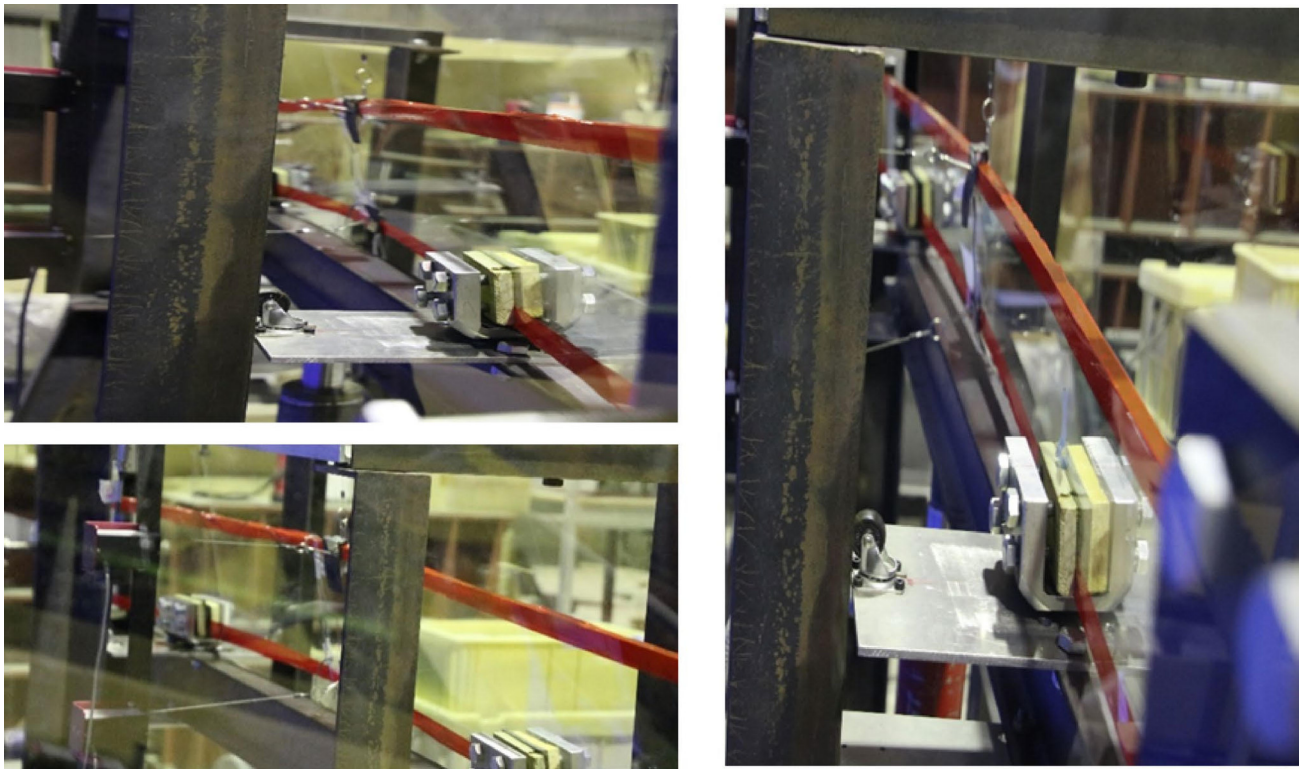

Fig. 6 Experimental observations of LTB mechanism (selection)

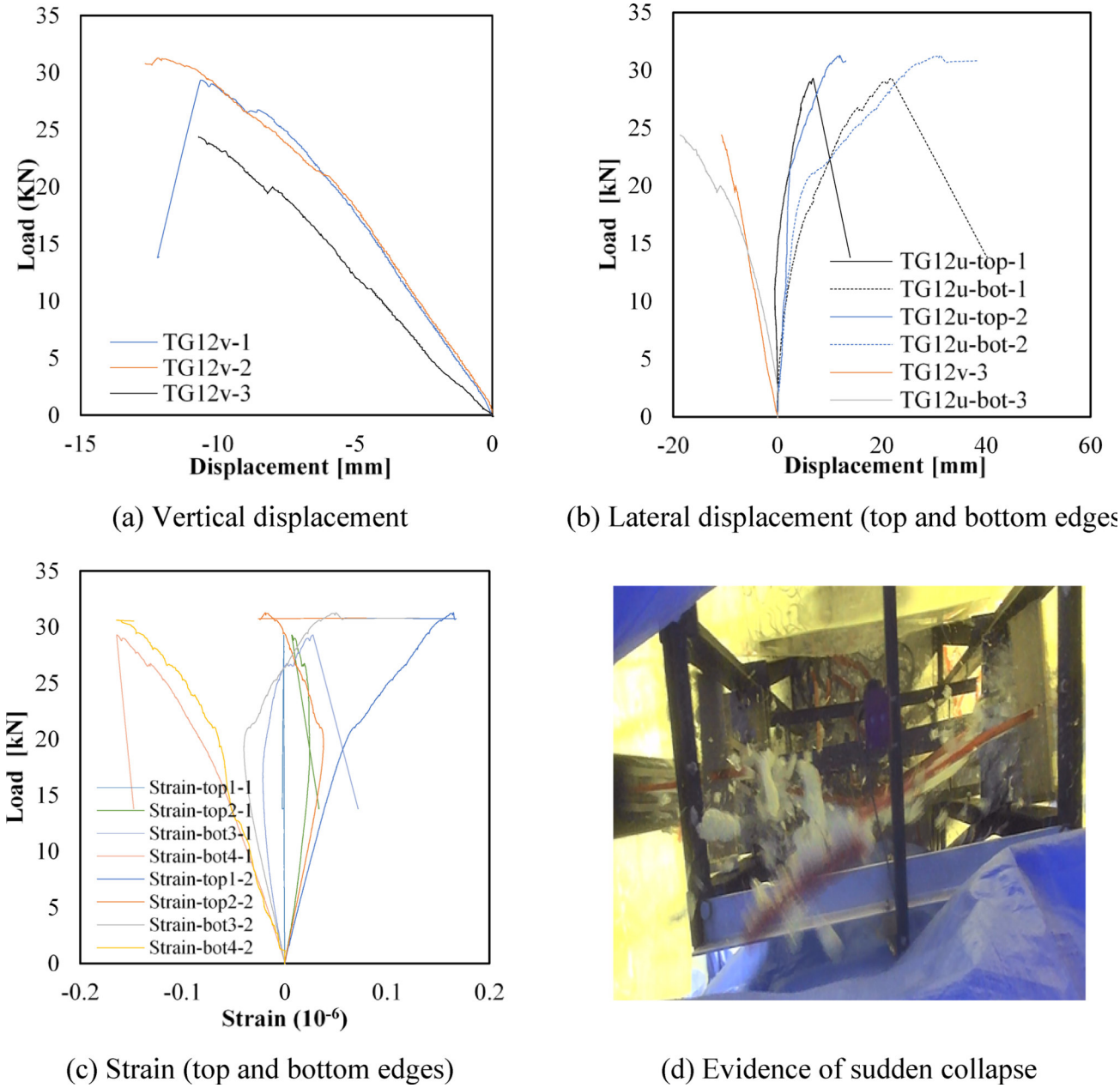

Fig. 7 Example of test results for the specimens with 12 mm thicknes

Table 2 Average of experimental outcomes. Specimens grouped by series and listed by slenderness

Series	Specimen	λ_{LT}	Displacement			Maximum load [kN]	Rotationφ [rad]
			Top-ver (v) [mm]	Hor (u_{top}) [mm]	Hor (u_{bot}) [mm]		
A	TG6-200	2.15	36.31	72.60	85.10	5.75	-0.062
	TG8-200	1.61	15.00	40.00	16.02	7.63	-0.119
	TG10-200	1.29	5.00	10.52	16.00	10.86	-0.030
B	TG8-150	1.12	10.40	2.65	18.75	12.40	-0.107
	TG12-200	0.93	6.40	0.30	21.40	30.10	-0.117
	TG8-130	0.71	18.50	32.10	14.50	12.13	-0.104
	TG10-180	0.48	6.32	0.60	26.34	10.65	-0.030

4 Elaboration of Test Results

4.1 Stress Ratio

Several significant facets of the structural behavior of single-layer tempered glass beams and panels under tensile and bending loads have been covered by experimental research. Tempered glass exhibits a brittle failure mechanism without plastic deformation before to rupture, in contrast to ductile materials like steel or aluminum. Failure happened abruptly and disastrously as soon as the applied tensile stress surpassed the material's inherent strength. This emphasizes how crucial it is to adopt adequate safety measures and precisely define acceptable stress levels when employing glass as the main load-bearing component in tensile constructions.

The bending behaviour of a beam, as known, is basically governed by a combination of tensile-to-compressive stresses at the extreme top/bottom edges of the resisting section. The determination of the tension-to-compression stress ratio at failure can thus represent an efficient tool to support the investigation of resisting mechanisms (initiation and progressive evolution) until failure.

For the present experiments, Table 3 shows the estimated stress ratios that are an integral part of the herein presented methodology, and provides insights about the way the member can respond to different loading regimes, particularly when the slenderness is small. The present study, in particular, proposes an average calibration of stress ratio, such that the tensile stress can be calculated as $\sigma_t = f_t(\overline{\sigma}_c)$, where $\overline{\sigma}_c$ is the maximum experimental compression stress (at failure).

The stress ratio γ introduced in Eq. (6), more in detail, was determined by averaging the collected experimental values for the 36 specimens belonging to series B of Table 1, being associated to a relatively low slenderness and (expected) small sensitivity to large LTB deflections (Table 2), but otherwise to a more pronounced inelastic mechanism with sudden and brittle collapse. To note that – from the original set of 10 available samples for each series – one of them was used for trial measurements, and thus not accounted for in the statistical analysis. Also, the 9th test for series TG8-130 was affected by the misleading track record of measures, and thus, it was disregarded for comparative calculations.

Table 3 Experimental determination of stress ratio g for type B specimens

No. of test in each series	Specimens			
	TG8-150 (λ_{LT}= 1.12)	TG12-200 (λ_{LT}= 0.93)	TG8-130 (λ_{LT}= 0.71)	TG10-180 (λ_{LT}= 0.48)
1	1.4067	0.4049	0.2044	2.1999
2	1.5526	0.2670	0.2238	0.4596
3	0.8487	0.5975	0.2266	0.6428
4	2.0302	0.2465	1.5569	0.1758
5	0.3333	0.4347	0.3290	0.1412
6	0.9444	0.6150	0.1155	0.5999
7	0.0895	0.6397	0.1955	0.1491
8	0.4382	0.5897	0.1355	0.5772
9	0.4963	0.1877	–	0.1751
Avg. (series)	0.9044	0.4425	0.374	0.5690
Avg. (type B)	0.5780			

The overall post-processing of experimental data, which is also briefly summarized in Table 3, resulted in about a final mean ratio γ=0.57 for the examined set of beam samples, that is:

$$\sigma_t = f_t(\overline{\sigma}_c) = \gamma \ \ \overline{\sigma}_c \ \approx \ 0.57 \ \overline{\sigma}_c \tag{6}$$

Notably, the final result of Eq. (6) is herein used to support the general methodology only. For this reason, the stress ratio g is preliminarily averaged from the available test results. On the other side, given the high variability of the collected experimental outcomes – as it can be perceived from Table 3 – it is clear that a more extended experimental database is necessarily required for a sound calibration of this key parameter.

4.2 Allowable Bending Stress

4.2.1 Statistical Analysis

From past experience and literature experiments, high slenderness ratios are demonstrated to be associated with an LTB response large displacements and elastic buckling, which is in line with Euler's buckling theory. Conversely, as in the present investigation (for example, Fig. 7d), a small slenderness ratio results in a progressively reduced deformation, with inelastic LTB and mostly sudden collapse, or even brittle failure, making this aspect crucial for design. Therefore, from a safety design perspective, it is essential to focus also on small slenderness ratios, due to the critical nature of the collapse mechanism.

In any case, it is also worth noting that the experimentally measured failure moment fluctuated significantly for each series of specimens, making statistical analysis necessary to determine trustworthy allowable stresses.

The presently elaborated statistical model, to this aim, applied a normal (symmetrical bell-shaped Gaussian) distribution and distinguished three specific cases/ranges of resisting mechanism and collapse based on slenderness, namely corresponding to (i) elastic buckling, (ii) inelastic buckling, and (iii) brittle collapse. The determination of the allowable bending stress for different failure mechanisms is crucial to guarantee structural safety against buckling, and thus also for the specific LTB case. Besides, while high

slenderness typically follows the Euler's theory, the present study aimed to mitigate the chance of brittle failure in glass beams with less pronounced susceptibility to elastic buckling.

The variability of the experimental buckling loads reported in Table 2 and illustrated in Fig. 9 appears approximately symmetric about the mean, indicating that the scatter of the present dataset is not strongly skewed. On this basis, a normal distribution was adopted to represent the statistical variability of the test results. Although alternative models such as Weibull or lognormal distributions are widely used for fracture strength analyses in large glass datasets, previous studies [31, 32] have shown that normal distributions can adequately describe the mechanical response of tempered glass, especially when the number of specimens is moderate. Accordingly, the assumption of normality was considered reasonable for the present study, providing a balanced representation of the average performance and dispersion. The basic assumption was to study the variation of bending stress at failure for the tested structural elements, and ensure, by applying statistical concepts, a 95% confidence level.

The probability density function of a normal distribution is given by:

$$f(x) = \frac{1}{\overline{\sigma}\sqrt{2\pi}} exp\left(-\frac{(\chi_{LT} - \mu)^2}{2\overline{\sigma_2}}\right) \tag{7}$$

The standard deviation $\overline{\sigma}$ measures the spread of the moment values around the mean value, calculated by taking the square root of the average squared deviations from the mean (Fig. 8).

The approach promotes structural safety improvement and stability by combining critical moment variance modifications with probabilistic modelling. A statistical approach is used to compute the lower limit parameter of the normal distribution curve, where:

$$C = \frac{(\chi_{LT} - \mu)}{\bar{\sigma}} \tag{8}$$

Generally, the standard normal distribution is $N\left(\chi_{LT}, \mu, \overline{\sigma}^2\right)$). The lower limit of the normal distribution curve is found by distributing the experimental data variance over each slenderness ratio, and the expression:

$$Z = \frac{\left(\frac{M_{cr}}{M_{res}} - \mu\right)}{\overline{\sigma}} \tag{9}$$

is used to ascertain the confidence interval C with a 95% confidence, where:

$$I(\infty \geq Z \geq C) = \int_0^{\infty} f(z)\,dz = 95\% \quad \Rightarrow \quad C = -1.6449 \tag{10}$$

To ensure that the maximum bending stress stays within safe limitations, the true mean bending stress is compared to the member average strength or design stress limits, using the upper and lower bounds provided by the computed confidence interval. Subsequently, it is suggested to estimate the ultimate bending moment of glass beams using M_{cr}, μ and $\overline{\sigma}$, as presently derived from in-plane loading experiments with a given set of specimens.

The computational approach assumes that:

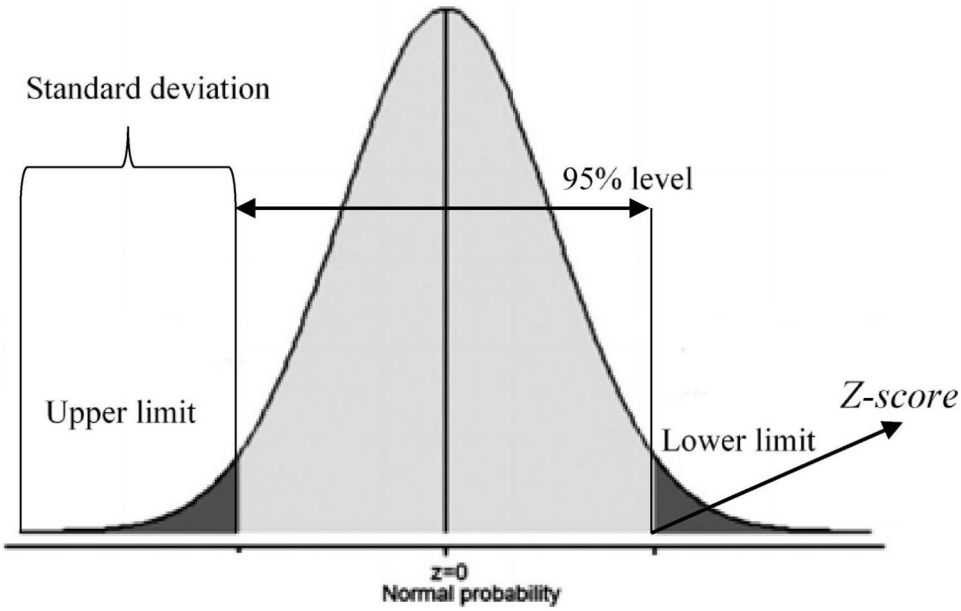

Fig. 8 Normal distribution curve (95% confidence level)

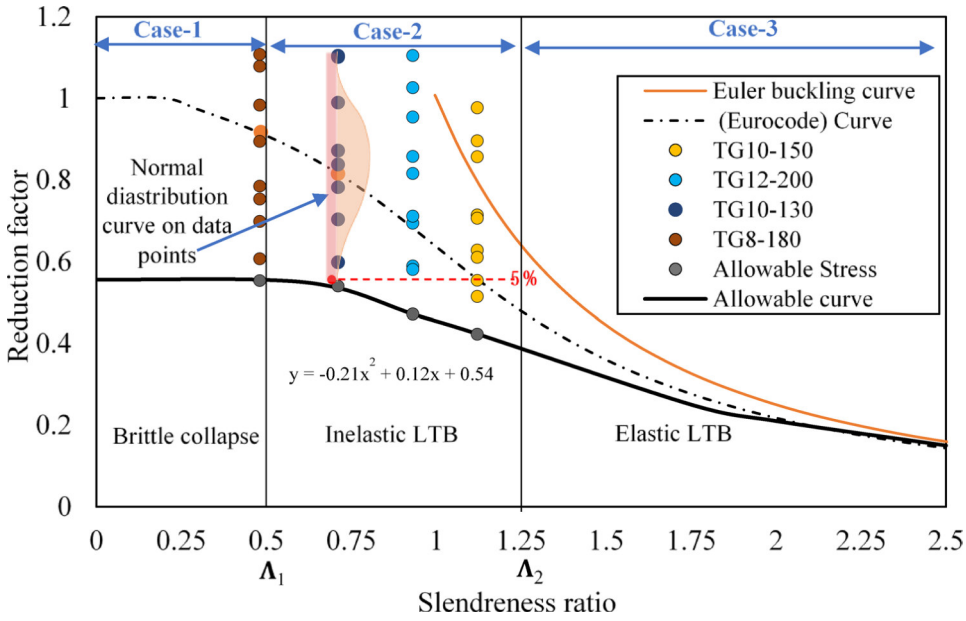

Fig. 9 Variance distribution of allowable stress with 95% confidence level

– the allowable/ultimate bending moment $\overline{M}_u$ should fall in a range of probability of 95%;
– the critical moment M_{cr} may be determined considering that $-1.6449 = (M_{cr}/M_{res} - \mu)/\overline{\sigma}$.

In conclusion:

$$\overline{M}_u = (\mu - 1.6449\overline{\sigma})\ M_{cr;avg} \tag{11}$$

can be used to calculate the reduction factor of $\overline{M}_u$, where $M_{cr;avg}$ accounts for the average critical moment from the available experimental data.

4.2.2 Results

For the present study, "allowable stress curve" is presented in non-dimensional form in Fig. 9, which gives evidence of the evolution of the reduction factor for the bending/buckling capacity of the examined members. Also, Fig. 9 emphasized three slenderness ratios (or ranges) that are specifically detected to satisfy the following limits:

– the calculated λ_{LT} falls in the first range, that is $\lambda_{LT} < \Lambda_1 = 0.5$ for beams with very high stiffness, very small slenderness, and sudden brittle failure;
– $\Lambda_1 = 0.5 \le \lambda_{LT} < \Lambda_2 = 1.25$ for beams with prevailing bending collapse and inelastic buckling; or.
– $\lambda_{LT} \ge \Lambda_2 = 1.25$ for beams that follow the Euler's buckling theory (elastic buckling).

In particular, the fitting expression in Fig. 9 is given by:

$$\chi_{LT} = -0.21\lambda_{LT}^2 + 0.12\lambda_{LT} + 0.54 \tag{12}$$

Table 4 Calculated reduction factors for critical and allowable bending moments, grouped by series/slenderness

Series	λ_{LT}	μ	$\overline{\sigma}$	Reduction factor for $M_{cr;avg}$	Reduction factor for $\overline{M}_u$
TG8-150	1.12	0.6714	0.151457	0.7179	0.4236
TG12-200	0.93	0.7638	0.176695	0.8153	0.4719
TG8-130	0.71	0.8555	0.183941	0.8425	0.5399
TG10-180	0.48	0.8862	0.161076	0.8663	0.5533

and is valid for the range $0.5 \le \lambda_{LT} < 1.25$.

Such a curve was conservatively obtained from the minimum values of the available experimental data (for the examined slenderness range of Type B specimens), by using the lower limit of 5% of normal distribution, based on the calculated *Z*-score. The curve in Eq. (12) was then extended and connected to the first and third slenderness cases/ranges, see Fig. 9. As it can be seen, the "allowable stress" curve approached the Euler's one for large slenderness, and intercepts the y-axis at about a≈0.55 reduction factor, based on statistical analysis.

In support of Fig. 9; Table 4 summarizes the mean (μ) and standard deviation ($\overline{\sigma}$) of critical moment variance for each examined slenderness ratio. The calculated reduction factor for the allowable bending moment ($\overline{M}_u$) also derives from the lowest limit of the normal distribution curve.

4.3 Basis for the Proposal of a General Allowable Bending Stress Formulation

In conclusion, the basis of a generalized methodology for calculating the allowable bending stress in glass beams is proposed [9], in analogy with research studies and literature proposals for other constructional materials [33–37].

4.3.1 Case 1: Brittle Behaviour ($\lambda_{LT} < \Lambda 1 = 0.5$)

When a member exhibits a mostly brittle collapse, substantial structural deformations do not take place before the sudden failure. Such a kind of failure mechanism is usual for materials with high strength but low ductility. Besides, specific considerations are required for glass members. In these hypotheses, the allowable bending stress should be limited to:

$$f_b \leq \alpha_L \gamma \overline{\sigma}_c \tag{13}$$

with:

γ = a suitable tension-to-compression stress ratio to derive from tests.

$\overline{\sigma}_c$ the maximum compression stress value (from tests).

α_L = environmental factor (to be quantified, based on experiments).

More in detail:

– Long-term allowable stress

$$f_{L,b} = \frac{1}{3}\alpha_L \gamma \overline{\sigma}_c \tag{14a}$$

– Short-term allowable stress

$$f_{s,b} = \frac{2}{3}\alpha_L \gamma \overline{\sigma}_c \tag{14b}$$

4.3.2 Case 2: Inelastic Critical Buckling ($\Lambda_1 = 0.5 \leq \lambda_{LT} < \Lambda_2 = 1.25$)

Before collapse, considerable elastic deformations usually occur for a member subjected to inelastic critical LTB. When the material can offer considerable flexibility and deformation capacity, and the slenderness ratio is still relatively low, this is the typically observed behaviour at failure. As such, the following inelastic buckling stress formula can be used:

$$\mathrm{f_b} = \sigma_t \lambda_{LT} = 0.57 \overline{\sigma}_c \ \lambda_{LT} \tag{15}$$

By using Eq. (15) and accounting for the previously described Eq. (12), it is possible to express:

$$f_b = 0.57 \overline{\sigma}_c \ \left(0.21 \lambda_{LT}^2 + 0.12 \lambda_{LT} + 0.54\right) \tag{16}$$

and thus:

– Long-term allowable stress.

$$f_{L,b} = \frac{1}{3} f_b \tag{17a}$$

– Short-term allowable stress

$$f_{s,b} = \frac{2}{3} f_b \tag{17b}$$

4.3.3 Case 3: Elastic Buckling ($\lambda_{LT} \geq \Lambda_2 = 1.25$)

Elastic buckling is the typical behaviour outcome of load-bearing members that bend elastically and are generally characterized by high slenderness. The Euler's buckling formula, adjusted for LTB, can be potentially employed to determine the critical stress.

This would result in:

– Long-term allowable stress

$$f_{L,b} = \frac{\pi \alpha_L}{3} \left(\frac{C_b}{W_x l_b} \sqrt{EI \ GJ} \right) \tag{18a}$$

– Short-term allowable stress

$$f_{s,b} = \frac{2\pi \alpha_s}{3} \left(\frac{C_b}{W_x l_b} \sqrt{EI \ GJ} \right) \tag{18b}$$

where the input parameters have been previously defined.

Allowable bending stresses for glass beams must be differentiated between short-term and long-term loading circumstances based on experimental data and statistical interpretation. In the presence of continuous loads, glass shows time-dependent behavior, especially when exposed to external factors including wind pressure, temperature changes, and creep effects in sealants or interlayers. For long-term applications, allowable stress levels must thus be lowered to accommodate sub-critical fault propagation and gradual fracture formation.

The basic tension ratio, which is the ratio of the applied stress to the intrinsic tensile capacity of tempered glass, including a safety factor, was proposed by Eq. 6. A baseline criteria for determining whether the applied demand stays within reasonable design bounds is provided by this ratio.

The allowable stress for brittle behavior, as stated in Eq. 13, is calculated by dividing the ultimate tensile strength by a suitable safety factor. The abrupt fracture mode seen in the trials, where no plastic redistribution of stresses is feasible, is reflected in this method. Therefore, it is especially important in situations involving short-term loads, such wind gusts or unintentional impacts, when the glass must withstand high demands without breaking.

The allowable stress formulation for inelastic behavior, as defined by Eq. 15, acknowledges that while glass is brittle

in and of itself, structural assemblies may exhibit a limited redistribution of stresses through neighboring panels, supporting frames, or sealants. This scenario provides a more realistic depiction of system behavior under service demands by calibrating the allowable stress to a lower value that takes partial stress sharing into account. This is especially important in situations with repetitive or quasi-static loads when redistribution mechanisms postpone catastrophic collapse. Finally, by limiting service stresses to remain firmly within the glass's linear elastic range, (Eq. 18a and 18b) determines the allowable stress for elastic behavior.

In summary, the differentiation between brittle, inelastic, and elastic assumptions provides a flexible framework for design. Short-term actions can be evaluated against brittle or inelastic formulations depending on the structural redundancy, while long-term loading must rely on elastic-based allowable stresses to ensure safety against delayed fracture. The proposed equations, therefore, enable designers to tailor the allowable bending stress to both the material behavior of glass and the nature of the applied load, ensuring consistency with experimental findings and statistical scatter at the 95% confidence level.

5 Conclusions and Future Work

The present research study experimentally investigated the in-plane bending and Lateral-Torsional Buckling (LTB) response of tempered glass beams such as TG8-150 (λ_{LT}= 0.93), TG12-200 (λ_{LT}= 0.93), TG8-130 (λ_{LT}= 0.71), TG10-180 (λ_{LT}= 0.48), analysing some key factors in their mechanical response, such as the bending stress evolution, the critical buckling moment, and the corresponding failure mechanism. Such an investigation was supported by 52 original samples, and the primary attention was specifically spent on beam specimens characterized by a small slenderness ratio (less than (λ=1.2), to address their inelastic LTB response.

The present research set out to find an effective method for calculating the allowable bending stress and moment (as well as its reduction factor 0.55) for glass members in bending configurations, as a function of their slenderness ratio. In this context, the study of experimental evidence received the majority of emphasis. After accounting for the moment variance of experimental results for a set of slenderness ratios that can be typically associated with inelastic LTB and sudden failure mechanism, the overall post-processing of experimental data, which is also briefly summarised in Table 3, produced a final mean ratio of γ=0.57 for the examined set of beam samples, which means $\sigma_t = f_t\left(\overline{\sigma}_c\right) = \gamma\ \ \overline{\sigma}_c\ \approx\ 0.57\ \overline{\sigma}_c$.

For post-processing of experimental results, a normal distribution with a 95% confidence level was used in the statistical analysis. Such an outcome was used for the preliminary assessment and development of a general methodology able to support the definition of allowable bending stress formulations.

As shown, the primary advantage of the present generalized proposal is that it considers the possible resisting mechanisms and failures for the long term and short term (including behaviour proposed the equcation brittle $f_b \le \alpha_L \gamma\, \overline{\sigma}_c$, inelastic $\mathrm{f_b} = \sigma_t \lambda_{LT} = 0.57\overline{\sigma}_c\ \lambda_{LT}$, or elastic LTB behaviours at collapse in Eq. 18a and 18b for the long-term and short-term loading, respectively) as a function of the slenderness ratio, which is used as a key input parameter. On the other side, however, the collected experimental outcomes also gave evidence of scattered results and suggest the need for a more extended experimental database, to support a sound and robust calibration of input parameters. In the future, the focus of research will be given to the experimental analysis of more configurations of technical interest, as well as to many additional influencing factors that could further affect the structural behaviour of similar members, including, for example, environmental factors or boundary and loading conditions.

Acknowledgements Japan Science and Technology (JST) SPRING (grant Number JPMJSP2154) funded a research project at Kyushu Institute of Technology – Building Structure Laboratory (Japan) and supported the scientific collaboration with the University of Trieste – Department of Engineering and Architecture (Italy).

Author Contributions Saddam Hussain: Writing—original draft, Software, Investigation, Formal analysis, Data curation. Pei Shan Chen: Writing—original draft, Supervision, Resources, Project administration, Funding acquisition. Chiara Bedon: Writing—original draft, Supervision, Data curation. Hassan Javed: Writing—original draft, Investigation.

Funding Open access funding provided by Università degli Studi di Trieste within the CRUI-CARE Agreement.

Declarations

Conflict of Interest The authors declare that they have no known competing financial interests or personal relationships that could have appeared to influence the work reported in this paper.

References

1. Apple Media Helpline (2019) Apple fifth avenue: the cube is back. https://www.apple.com/newsroom/2019/09/apple-fifth-avenue-the-cube-is-back/
2. Allen E (2015) The most innovative glass buildings. https://www.architecturaldigest.com/gallery/the-most-innovative-glass-buildings
3. Hussain S, Chen P-S, Koizumi N, Liu B, Yan X (2023) Experimental study on spring constants of structural glass panel joints under in-plane loading. Pertanika J Sci Technol. https://doi.org/10.47836/pjst.31.4.21
4. Hussain S, Bedon C, Kumar G, Ahmed Z (2023) Bayesian regularization backpropagation neural network for glass beams in lateral–torsional buckling. Adv Civil Eng 2023:11. https://doi.org/10.1155/2023/6619208
5. Chen PS (2008) A study report on an ancient wood bridge Hongqiao. Struct Eng Int 2:84–87
6. Chen PS (2012) Introduction to 1.5-layer space frames. Proceedings of IASS annual symposium: IASS-APCS: 2012. Korean Society of Spatial Structure, Seoul, p 467–474
7. Chen PS (2012) A report on the innovation of reciprocal panel system. Proceedings of IASS annual symposium: IASS-APCS: 2012. Korean Society of Spatial Structure, Seoul, p 491–495
8. Chen PS, Tsai M-T (2019) On configuration and structural design of frameless glass structures. In: Structures and architecture – bridging the gap and crossing borders. CRC Press, pp 10 (ISBN 9781315229126)
9. JSCE – Japan Society of Civil Engineers (2007) Standard specifications for steel and composite structures (ISBN: 978-4-8106-0565-5)
10. Kato B (1988) Design rules for connections in Japan. J Constr Steel Res 10:357–374
11. Hussain S, Chen PS, Bedon C, Javed H (2024) Promoting the allowable stress method for the design of glass members and frameless structures. Proceedings of international exchange and innovation conference on engineering & sciences (IEICES), p 943–949
12. European Committee for Standardization (CEN) EN 1993-1-1 (2005) Eurocode 3: design of steel structures. Part 1–1: general rules and rules for buildings. Brussels
13. Pešek O, Melcher J (2018) Lateral-Torsional buckling of structural glass beams. Exp Study Procedia Eng 190:70–77
14. Amadio C, Bedon C (2010) Buckling of laminated glass elements in out-of-plane bending. Eng Struct 32:3780–3788
15. Amadio C, Bedon C (2013) A buckling verification approach for monolithic and laminated glass elements under combined in-plane compression and bending. Eng Struct 52:220–229
16. Bedon C, Amadio C (2015) Design buckling curves for glass columns and beams. ICE Proc Struct Build 168(7):514–526
17. Bedon C, Amadio C (2014) Flexural-torsional buckling: experimental analysis of laminated glass elements. Eng Struct 73(8):85–99
18. Hussain S, Chen P-S, Hassanlou D, Bolhassani M, Bedon C (2024) Bending and lateral-torsional buckling investigation on glass beams for frameless domes. Results Eng 21:101962. https://doi.org/10.1016/j.rineng.2024.101962
19. Ferreira GNA (2022) Design of Multi-Layered laminated glass beams in Lateral-Torsional buckling. Int J Struct Glass Adv Mater Res 6(1):23–32. https://doi.org/10.3844/sgamrsp.2022.23.32
20. Blaauwendraad J (2007) Buckling of laminated glass columns. Heron 52:147–218
21. Bedon C, Amadio C (2016) A unified approach for the shear buckling design of structural glass walls with non-ideal restraints. Am J Eng Appl Sci 9(1):64–78
22. Bedon C, Amadio C (2014) Buckling analysis of simply supported flat glass panels subjected to combined in-plane uniaxial compressive and edgewise shear loads. Eng Struct 59:127–140
23. López-Aenlle M, Pelayo F, Ismael G, Garcia Prieto MA, Martin Rodriguez A, Fernandez-Canteli A (2016) Buckling of laminated-glass beams using the effective-thickness concept. Compos Struct 137:44–55
24. Setti Barroso V, Andrade A, Providencia P, Challamel N (2023) A von Kármán-type model for two-layer laminated glass plates, with applications to buckling and free vibration under in-plane edge loads. Compos Struct 322:117287
25. Chen P-S, Hussain S, Matsuno Y (2023) Experimental report on glass panels against static and repeated in-plane compression loading. J Struct Eng 69B:225–231. https://doi.org/10.3130/aijjse.69B.0_225
26. Teke Tebo E-P, Masu L, Nziu P (2020) Effects of factors that influence out-of-plane lateral-torsional buckling of freestanding circular arches. J Eng 2020:ArticleID4892070–12pages
27. Ozbasaran H, Aydin R, Dogan M (2015) An alternative design procedure for lateral-torsional buckling of cantilever I-beams. Thin-Walled Struct 90:235–242
28. Silva de Carvalho A, Martins CH, Moura de Oliveira V, Rossi A (2023) Proposal of modification of the factor to non-uniform bending moment by artificial intelligence. Proceedings of the 20th international conference on experimental mechanics, Porto, Portugal
29. Barnat J, Bajer M, Vild M, Melcher J, Karmazinova M, Pijak J (2017) Experimental analysis of lateral torsional buckling of beams with selected cross-section types. Proceedings of the 18th international conference on rehabilitation and reconstruction of buildings (CRRB 2016). Procedia Engineering, vol 195, p 56–61
30. Zhang W, Liu F, Xi F (2018) Lateral torsional buckling of steel beams under transverse impact loading. Shock Vib 2018:15
31. Haldimann M, Luible A, Overend M (2008) Structural use of glass. International association for bridge and structural engineering
32. Galuppi L, Royer-Carfagni G (2012) The effective thickness of laminated glass plates. J Mech Mater Struct 7(4):375–400
33. Katabira K, Kurita H, Mori K, Tamura H, Narita F (2023) Monitoring of allowable bending stress overload in glass-fiber-reinforced polymer composites using magnetostrictive Fe–Co fibers. Adv Eng Mater 26(4):2300529
34. Pang S-J, Lee J-J, Oh J-K (2013) Evaluation of allowable bending stress of dimension lumber; confidence levels and size-adjustment. J Korean Wood Sci Tech 41(5):432–439
35. Jung K, Nakamine S (2006) Development of a hybrid pin joint with a compressed wooden dowel and metal pipe. Open J Civil Eng 5(1)
36. Tada M, Fukui T, Nakashima M, Roeder CW (2003) Comparison of strength capacity for steel Building structures in the United States and Japan. Earthq Eng Eng Seismol 4(1):37–49
37. Sasaki Y, Yamasaki M, Uchida M, Torichigai T (2014) Non-destructive stress evaluation of wood members in Japanese traditional buildings. Proceedings of the 11th European conference on non-destructive testing (ECNDT 2014), 8 pages, October 6–10, Prague, Czech Republic